

Article

Comparison of Adsorbents for Cesium and Strontium in Different Solutions

Shengnan Fan ¹, Lu Jiang ¹, Zhiqian Jia ^{1,*}, Yu Yang ^{2,*} and Li'an Hou ²¹ College of Chemistry, Beijing Normal University, Beijing 100875, China² School of Environment, Beijing Normal University, Beijing 100875, China

* Correspondence: zhqjia@bnu.edu.cn (Z.J.); yangyu@bnu.edu.cn (Y.Y.)

Abstract: Adsorption is an effective method to remove cesium and strontium from a solution. Although a variety of adsorbents has been reported, it is difficult to compare their adsorption properties due to different experimental conditions (such as solution concentration, volume, composition, temperature, etc.). In this paper, a series of adsorbents for the adsorption of cesium and strontium (ammonium phosphomolybdate, Prussian blue, sabite, clinoptilolite, titanium silicate) were synthesized and characterized using XRD, IR and SEM, and their adsorption performance in mixed solution (containing Li, Na, K, Cs, Ca, Sr and Mg ions, 1 mmol L⁻¹), artificial seawater and salt lake brine were studied under the same conditions; in addition, the adsorption mechanism was elucidated. The results showed that ammonium phosphomolybdate has the largest adsorption capacity for cesium in the mixed solution. In artificial seawater and salt lake brine, Prussian blue displays the highest cesium adsorption capacity and the best selectivity. The multi-adsorption mechanisms are beneficial to the selective adsorption of Prussian blue in complex solutions. These results are useful for choosing adsorbents for cesium and strontium in applications.

Keywords: adsorption; cesium; chabazite; clinoptilolite; phosphomolybdate; Prussian blue; strontium



Citation: Fan, S.; Jiang, L.; Jia, Z.; Yang, Y.; Hou, L. Comparison of Adsorbents for Cesium and Strontium in Different Solutions. *Separations* **2023**, *10*, 266. <https://doi.org/10.3390/separations10040266>

Academic Editor: Mingheng Li

Received: 22 March 2023

Revised: 3 April 2023

Accepted: 13 April 2023

Published: 19 April 2023



Copyright: © 2023 by the authors. Licensee MDPI, Basel, Switzerland. This article is an open access article distributed under the terms and conditions of the Creative Commons Attribution (CC BY) license (<https://creativecommons.org/licenses/by/4.0/>).

1. Introduction

Nuclear energy has developed rapidly in the past few decades and provides an important kind of energy for the increasing demands of mankind. However, the cesium and strontium produced by nuclear power plants emit extremely high gamma radiation and fission yields. Improper disposal of nuclear waste will result in the release of radionuclides into the environment. The main ways for radioactive materials to enter the human body include drinking water contaminated with radioactive water, eating fish cultured in water bodies contaminated with radioactive water, and eating crops irrigated by water bodies contaminated with radioactive water [1,2]. Cesium and strontium can easily enter the human body through the food cycle, causing serious adverse effects on human health and environment. Therefore, the removal of cesium and strontium from nuclear waste water has become a research hotspot. On the other hand, as a highly dispersed metal element, cesium usually coexists with other alkali metals in the salt lakes, geothermal waters and oil field brines under natural conditions [3,4]. Separation of cesium from other alkali metals is one of the most difficult problems due to their close similarity in physical and chemical properties [5,6].

The methods for removing cesium and strontium include chemical precipitation, solvent extraction, evaporation and adsorption [7]. Among them, adsorption is considered an effective and cost-effective method [8,9]. Many kinds of adsorbents for cesium and strontium have been reported in the literature, such as ammonium phosphomolybdate (AMP) [10], ferric ferrocyanide (PB) [11], chabazite (CBT) [12], clinoptilolite (CPT) [13] and sodium titanium silicate (CST) [14]. For example, herschelite was used for the removal of Cs to treat the highly contaminated water at Fukushima Daiichi Nuclear Power Station

(seawater was injected into the reactors to cool the damaged reactor core) [15]. At Three Mile Island Unit 2 (TMI-2), chabazite and A-type zeolite were packed into a vessel to remove radioactive Cs and Sr from water contaminated by the nuclear accident [16].

Nevertheless, due to the different adsorption conditions (e.g., solution concentration, volume, composition, temperature, adsorbent amount, etc.), it is difficult to compare the adsorption performance of different adsorbents reported by different laboratories, resulting in difficulty in choosing adsorbents. In this paper, a series of adsorbents were synthesized, and their adsorption performance for cesium and strontium in mixed solutions (containing Li, Na, K, Cs, Ca, Sr, and Mg ions, 1 mmol L^{-1}), artificial seawater and salt lake brine was studied, under the same conditions, and the adsorption mechanism was elucidated. These results are helpful for choosing adsorbents for cesium and strontium in applications.

2. Experimental Section

2.1. Materials

Ammonia chloride, ferric trichloride, potassium hexacyanoferrate, sodium hydroxide, sodium chloride, anhydrous calcium chloride, magnesium chloride hexahydrate, lithium chloride, potassium chloride, cesium chloride, TLC silica gel, aluminum foil, clinoptilolite, tetrabutyl titanate (97%), and tetrabutyl orthosilicate (99%) were of analytical grade and purchased from Beijing Chemical Plant (Beijing, China).

2.2. Preparation of AMP

A total of 9.13 g phosphomolybdic acid was used to prepare 25 mL of 0.2 mol L^{-1} phosphomolybdic acid solution. In total, 25 mL of 0.2 mol L^{-1} ammonium chloride solution was added in phosphomolybdate solution and reacted for 2 h under stirring. Ammonium phosphomolybdate precipitate was obtained and dried at $80 \text{ }^\circ\text{C}$ in vacuum for 12 h.

2.3. Preparation of PB

A total of 2.16 g FeCl_3 was used to prepare 200 mL of 0.04 mol L^{-1} FeCl_3 solution, and a certain amount of hydrochloric acid was added to prevent hydrolysis. In total, 1.69 g $\text{K}_4\text{Fe}(\text{CN})_6$ was weighed to prepare 20 mL of 0.2 mol L^{-1} $\text{K}_4\text{Fe}(\text{CN})_6$ solution. $\text{K}_4\text{Fe}(\text{CN})_6$ solution was added to FeCl_3 solution drop by drop under stirring and reacted for 2 h. The precipitate was centrifuged, washed with distilled water for three times, and then dried at $80 \text{ }^\circ\text{C}$ in vacuum for 12 h.

2.4. Preparation of CBT

Aluminum foil measuring $5.4 \times 10^{-2} \text{ g}$ was weighed and dissolved in 0.4 mL of 24 mol L^{-1} KOH, and stirred for 10 min. A total of 5 mL of water and 0.6 g of TLC silica gel were added and stirred for 10 min. In total, 4.6 mL water was added and stirred. The molar ratio was $10 \text{ SiO}_2: \text{Al}_2\text{O}_3: 4.8 \text{ K}_2\text{O}: 600 \text{ H}_2\text{O}$. Finally, the gel was transferred to a stainless steel reactor lined with polytetrafluoroethylene and crystallized at $110 \text{ }^\circ\text{C}$ for 5 days. The product was washed and dried.

2.5. Modification of CPT

Natural clinoptilolite (200 mesh) was added in pure water and washed, then the supernatant was removed and the precipitate was dried at $120 \text{ }^\circ\text{C}$. A total of 30 g clinoptilolite was added to 300 mL of 2 mol L^{-1} NaCl solution, and stirred at $80 \text{ }^\circ\text{C}$ for 24 h. The supernatant was removed, and the precipitate was washed with pure water and dried at $80 \text{ }^\circ\text{C}$ in vacuum for 10 h.

2.6. Preparation of CST

A total of 78 mL of 6 mol L^{-1} NaOH solution was added to a mixture of 13.6 g tetrabutyl titanate and 10 g tetrabutyl orthosilicate, and reacted at $150 \text{ }^\circ\text{C}$ for five days. The precipitate was washed with distilled water and ethanol, and then dried at $100 \text{ }^\circ\text{C}$.

2.7. Adsorption in Mixed Solution

A mixed chlorides solution containing Li, Na, K, Cs, Ca, Sr and Mg with respective concentration of 1 mmol L^{-1} was prepared. A total of 0.1 g of adsorbent was added to 50 mL of the mixed solution, and stirred for 12 h. The concentrations of Cs, Li, Na, K, Ca, Sr and Mg were determined using ICP-OES and ICP-MS.

2.8. Adsorption in Artificial Seawater

The artificial seawater was prepared according to the components of seawater of the southeast coast of China (provided by the Marine Biochemistry Laboratory of the Third Institute of Oceanography, State Oceanic Administration of China, Xiamen, China). The artificial seawater contains NaCl 26.518 g L^{-1} , MgSO_4 3.305 g L^{-1} , MgCl_2 2.447 g L^{-1} , CaCl_2 1.141 g L^{-1} , KCl 0.725 g L^{-1} , NaHCO_3 0.202 g L^{-1} , and NaBr 0.083 g L^{-1} . CsCl and SrCl_2 were also added in the artificial seawater for adsorption (CsCl and SrCl_2 concentration of 0.001 mol L^{-1}). A total of 0.1 g ammonium phosphomolybdic acid, Prussian blue, chabazite and clinoptilolite were added in 50 mL of the artificial seawater, and stirred for 12 h. The concentration of strontium and cesium was determined using ICP-OES and ICP-MS.

2.9. Adsorption in Salt Lake Brine

Salt lake brine (Qinghai, China) contains Li, Na, K, Rb and Cs with concentrations of 5488, 1879.5, 763.5, 0.0331, 0.0305 mg L^{-1} , respectively. A total of 0.05 g of ammonium phosphomolybdate, Prussian blue, chabazite and clinoptilolite was added in 25 mL of salt lake brine, respectively. The concentrations of Li, Na, K, Rb and Cs were determined using ICP-MS (NexION 300X, PerkinElmer, Waltham, MA, USA).

2.10. Characterization

The phase structure of adsorbents was analyzed using an X-ray powder diffractometer (XRD, X'Pert Pro MPD, Panalytical, Almelo, The Netherlands). The morphology of adsorbents was observed with a scanning electron microscope (SEM, S-4800, Hitachi, Tokyo, Japan). The chemical structure was detected with a Fourier-transform infrared spectrophotometer (FTIR, Affinity-1, Shimadzu, Kyoto, Japan).

3. Results and Discussion

3.1. Characterization of Adsorbents

Figure 1a shows the XRD patterns of AMP, with diffraction peaks at 10.8° , 15.2° , 21.6° , 26.5° , 30.7° , 36.1° and 55.7° , corresponding to 110, 200, 220, 222, 400, 332 and 550 crystal planes (card No.46-1405, p-space group) [17]. PB powder shows peaks at 17.5° , 24.8° , 35.4° , 39.8° , 43.7° , 50.9° , 54.3° and 57.5° (Figure 1b), corresponding to 200, 220, 400, 420, 422, 440, 600 and 620 crystal planes [18]. Figure 1c shows the XRD patterns of the prepared chabazite, and the peaks are consistent with the standard XRD patterns, while the peak intensity and width are wider, indicating that the prepared chabazite is small in size. Chabazite powder shows peaks at 12.85° , 13.91° , 15.98° , 17.67° , 19.03° , 20.57° , 21.93° , 22.27° , 24.83° , 25.78° , 27.43° , 28.00° , 30.37° and 33.39° , corresponding to 110, 012, 012, 003, 202, 211, 113, 300, 104, 220, 131, 024, 401 and 205 crystal planes [19]. Clinoptilolite powder shows peaks at 9.89° , 13.42° , 22.19° , 26.75° , 30.05° , 36.25° , 42.52° , 50.24° and 60.08° (Figure 1d), corresponding to 020, 031, 320, 313, 044, 112, 211, 220 and 311. Titanium silicate shows peaks at 11.3° , 14.8° , 17.7° , 26.6° , 27.6° , 34.5° , 36.4° and 45.5° , corresponding to crystal planes of 100, 002, 111, 211, 113, 300, 310 and 606 [20].

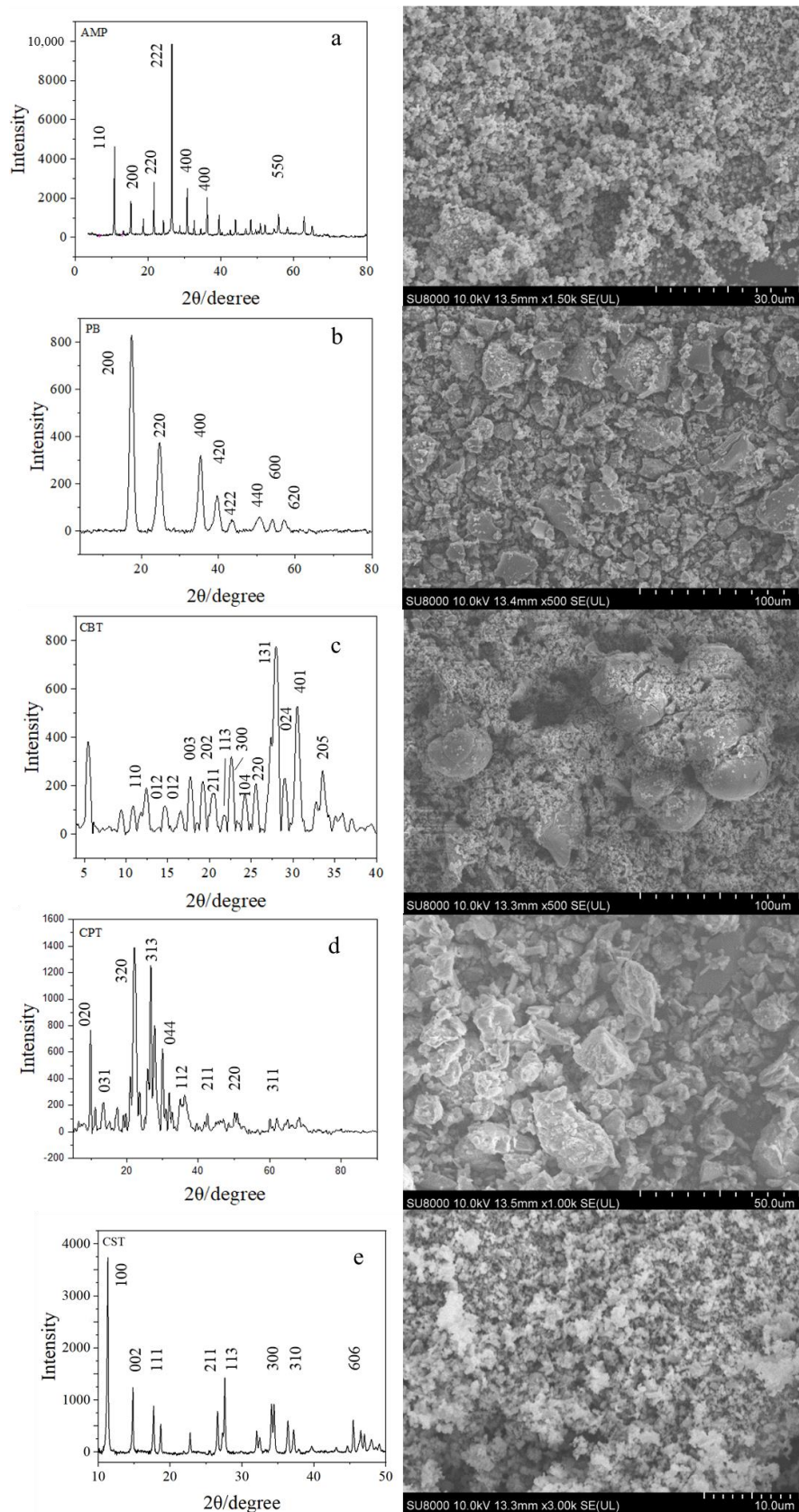


Figure 1. Powder X-ray diffraction patterns and SEM images of as-obtained adsorbents. (a). AMP (b). PB (c). Chabazite (d). Clinoptilolite (e). Titanium silicate.

Figure 1 shows the SEM images of the adsorbents. It can be seen that the AMP particles obtained using the direct precipitation method are relatively uniform, measuring approximately 0.5 μm in size. The PB particles are approximately 1–2 μm, with some aggregates of 10–20 μm in size. The as-prepared chabazite consists of small particles with an average diameter of 0.5 μm. Clinoptilolite is irregular, measuring approximately 10 μm in size. Titanium silicate are spherical particles with diameter of approximately 100 nm. According to Scheller’s formula [21],

$$D = \frac{K \gamma}{B \cos \theta} \tag{1}$$

where D is the average grain size, K is the Scherrer constant, γ is the X-ray wavelength, B is the half-height width of the diffraction peak, and θ is the Bragg diffraction angle. The calculated grain diameter of AMP is approximately 2 nm, that of Prussian blue is approximately 45 nm, that of chabazite is 2.72 nm, that of clinoptilolite is 3 nm, and that of sodium titanosilicate is approximately 1.74 nm.

As shown in Figure 2a, in the IR spectra of AMP, 3423 cm⁻¹ and 1630 cm⁻¹ come from the H-O-H vibration, and 3200 cm⁻¹ and 1604 cm⁻¹ are from the N-H vibration. The bands at 1062 cm⁻¹, 964 cm⁻¹, 865 cm⁻¹ and 786 cm⁻¹ are the characteristic absorption of the internal Keggin structure of [PMo₁₂O₄₀]³⁻. In Figure 2b, 3400 cm⁻¹ and 1606 cm⁻¹ are ascribed to the H-O-H vibration in PB, and 2080 cm⁻¹ and 499 cm⁻¹ are -C≡N- and Fe⁺-CN-Fe⁺ vibration. In Figure 2c, 3453 cm⁻¹ and 1612 cm⁻¹ are from H-O-H vibration in CBT, and 1405 cm⁻¹ and 1020 cm⁻¹ are the stretching vibration of Si-O-Si and Si-O-Al, and 721 cm⁻¹ and 611 cm⁻¹ the vibration of O-Si-O, and 470 cm⁻¹ is the bending vibration of O-Si-O and the double six-member ring vibration. In Figure 2d, 1205 cm⁻¹ and 1062 cm⁻¹ are the asymmetric stretching vibration of T-O-T (T=Si or Ti) in CPT, and 790 cm⁻¹ is the stretching vibration of O-T-O, and 600 cm⁻¹ is the coupling vibration of tetrahedral double ring. In Figure 2e, 966 cm⁻¹ is the stretching vibration of Si-O-Ti, and 902 cm⁻¹ is the vibration of the tetrahedron of Si-O, and 588 cm⁻¹ and 437 cm⁻¹ are the Ti-O bending vibration.

3.2. Adsorption in Mixed Solution

In the mixed solution of 1 mmol L⁻¹ of CsCl, LiCl, NaCl, KCl, CaCl₂, SrCl₂ and MgCl₂, the concentration of Cs, Li, Na, K, Ca, Sr and Mg is 0.001 mol L⁻¹, and the Cl concentration is 0.008 mol L⁻¹. The ionic strength is expressed as follows:

$$I = \frac{1}{2} \sum_{i=1}^n c_i z_i^2 \tag{2}$$

where I is the ionic strength, C_i is the ion concentration, z_i is the ion charge. The ionic strength was calculated to be 0.006 mol L⁻¹, which is less than 0.1 mol L⁻¹. Therefore, the mixed solution can be regarded as a dilute solution. The mixed solution was adsorbed with adsorbents under stirring for 12 h, and the adsorption amount is expressed as follows:

$$Q_e = \frac{(C_0 - C_e) \times v_0}{w_0} \tag{3}$$

where Q_e (mg g⁻¹) is the adsorption amount, C₀ (mg L⁻¹) is the initial concentration, C_e (mg L⁻¹) is the concentration after adsorption, V₀ (L) is the volume of the mixed solution, and W₀ (g) is the mass of adsorbent. The distribution coefficient K_d of ion in the adsorbent and solution is defined as follows:

$$K_d = \frac{(C_0 - C_e)V_0}{C_e w_0} = \frac{Q_e}{C_e} \tag{4}$$

In order to evaluate the adsorption selectivity of adsorbents, the separation factor is defined as follows:

$$\beta = \frac{Q_{e,Cs} \cdot C_{X,e}}{Q_{e,X} \cdot C_{Cs,e}} = \frac{K_{d,Cs}}{K_{d,X}} \tag{5}$$

where $Q_{e,Cs}$ and $Q_{e,X}$ are the adsorption amount of cesium and other ions, C_{Cs} and C_X are the residual concentration of cesium and other ions in the solution, $K_{d,Cs}$ and $K_{d,X}$ are the distribution coefficients of cesium and other ions, respectively. It should be noted that potassium compounds are used in the preparation of PB and CBT, and sodium compounds are employed in the preparation of CPT and CST, which may result in the residual K or Na in the compounds. Therefore, to prevent errors, K^+ adsorption is not considered for PB and CBT, and Na^+ adsorption is not calculated for CPT and CST.

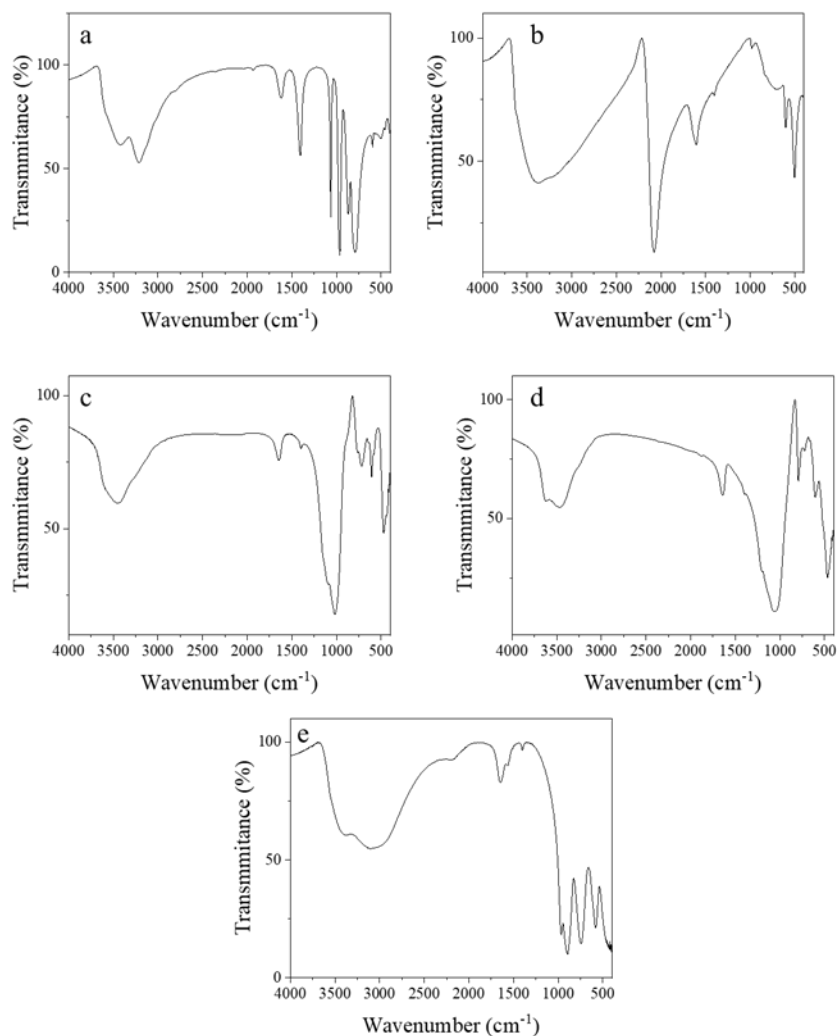


Figure 2. FT-IR spectra of adsorbents (a). AMP (b). PB (c). CBT (d). CPT (e). CST.

As shown in Figure 3a, the order of adsorption amount of adsorbents for cesium is as follows: AMP (62.88 mg g^{-1}) > CBT (50.51 mg g^{-1}) > CPT (42.97 mg g^{-1}) > PB (37.93 mg g^{-1}) > CST (13.41 mg g^{-1}). The distribution coefficients of AMP for K, Ca, Mg, Sr and Cs are 0.025, 0.046, 0.035, 0.063 and 43.36. The distribution coefficients of chabazite for Li, Na, Ca, Mg, Sr and Cs are 0.018, 0.045, 0.12, 0.035, 0.27 and 1.93. For clinoptilolite, the distribution coefficients of K, Ca, Mg, Sr and Cs are 0.11, 0.036, 0.0025, 0.13 and 1.04. The distribution coefficients of sodium tinosilicate for Li, K, Ca, Mg, Sr and Cs are 0.54, 1.51, 24.68, 1.36, 13.73 and 0.13.

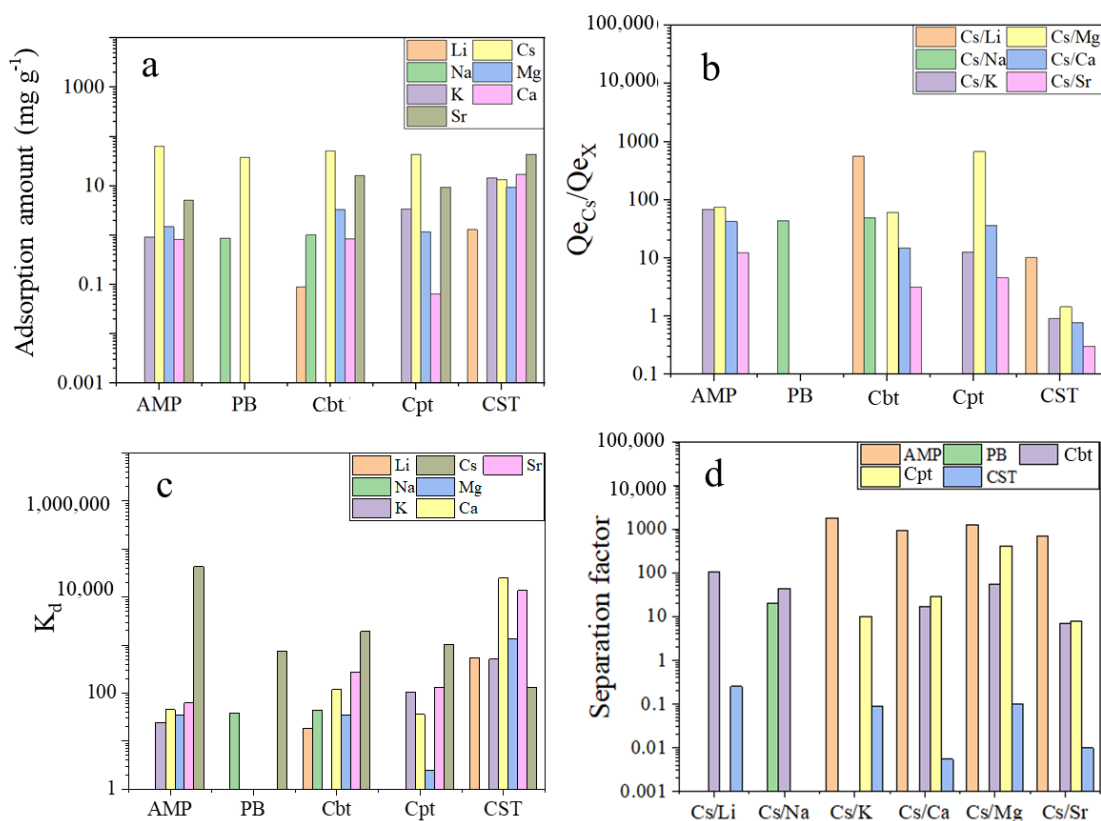


Figure 3. (a). Adsorption amount of adsorbents in mixed solution. (b). Ratio of adsorption amount of cesium to other elements. (c). Distribution coefficient. (d). Separation factor.

The separation factors of Cs to K, Ca, Mg and Sr in AMP adsorption are 1767.59, 945.90, 1242.25 and 687.34, respectively. The separation factor of Cs to Na in PB adsorption is 19.75. In CBT adsorption, the separation factors of Cs to Li, Na, Ca, Mg and Sr are 104.45, 43.05, 16.47, 54.86 and 7.06, respectively. The separation factors of Cs to K, Ca, Mg and Sr in CPT adsorption are 9.91, 29.25, 414.01 and 7.95, respectively. In CST adsorption, the separation factors of Cs to Li, K, Ca, Mg and Sr are 0.25, 0.088, 0.0054, 0.098 and 0.0097, respectively. It can be seen that AMP, PB, CBT and CPT display better selectivity for Cs, and titanium silicate has the best selectivity for strontium.

3.3. Adsorption in Artificial Seawater

In the artificial seawater, the concentration of Na, Mg, Ca, K, Cs, and Sr is 0.457, 0.0532, 0.0103, 0.0097, 0.001 and 0.001 mol L⁻¹ and the concentration of Cl, SO₄²⁻, HCO₃⁻, and Br⁻ is 0.538, 0.0275, 0.0024 and 0.0008 mol L⁻¹, respectively.

Adsorbents were used for adsorption in the artificial seawater under stirring for 12 h. The adsorption results are shown in Figure 4. The order of adsorption amount for cesium is as follows: Prussian blue (49.84 mg g⁻¹) > ammonium phosphomolybdate (32.51 mg g⁻¹) > chabazite (19.11 mg g⁻¹) > clinoptilolite (8.82 mg g⁻¹). Compared with the adsorption in the mixed solution, the adsorption amount of cesium on adsorbents, except for PB, is lower in the artificial seawater. The adsorption capacity for strontium also decreases significantly, and only the chabazite and titanium silicate exhibit significant adsorption for strontium, with an adsorption amount of 0.40 mg g⁻¹ and 20.60 mg g⁻¹, respectively.

The ionic strength of the artificial seawater is 0.688 mol L⁻¹, which is 115 times that of the mixed solution. With the increase in ionic strength, the electrostatic interaction between solution and adsorbent weakens. The adsorption mechanism of chabazite and clinoptilolite is mainly controlled by the electrostatic interaction between the adsorbent and ions, resulting in the reduced adsorption amount of the two adsorbents in the artificial seawater [19,22]. Prussian blue shows the highest adsorption capacity due to the multiple

adsorption mechanisms, including ion exchange and defects capturing of Prussian blue for cesium. Hijikata et al., also found that [15] from the equilibrium ion-exchange isotherms of herschelite, the adsorption of Cs is hampered by the existence of sea salt, and the adsorbed amount of Cs decreases from 5.7×10^{-2} to 4.2×10^{-3} mmol g⁻¹ at 1000 bed volume with an increase in the sea salt ratio in the feed solution from 0 to 3.4 wt%. The selectivity of sodium titanium silicate to strontium in simulated seawater is obviously increased because the alkaline environment is conducive to the selection of sodium titanosilicate to strontium. The simulated seawater PH value is generally between 7.8 and 8.5, showing weak alkalinity [23].

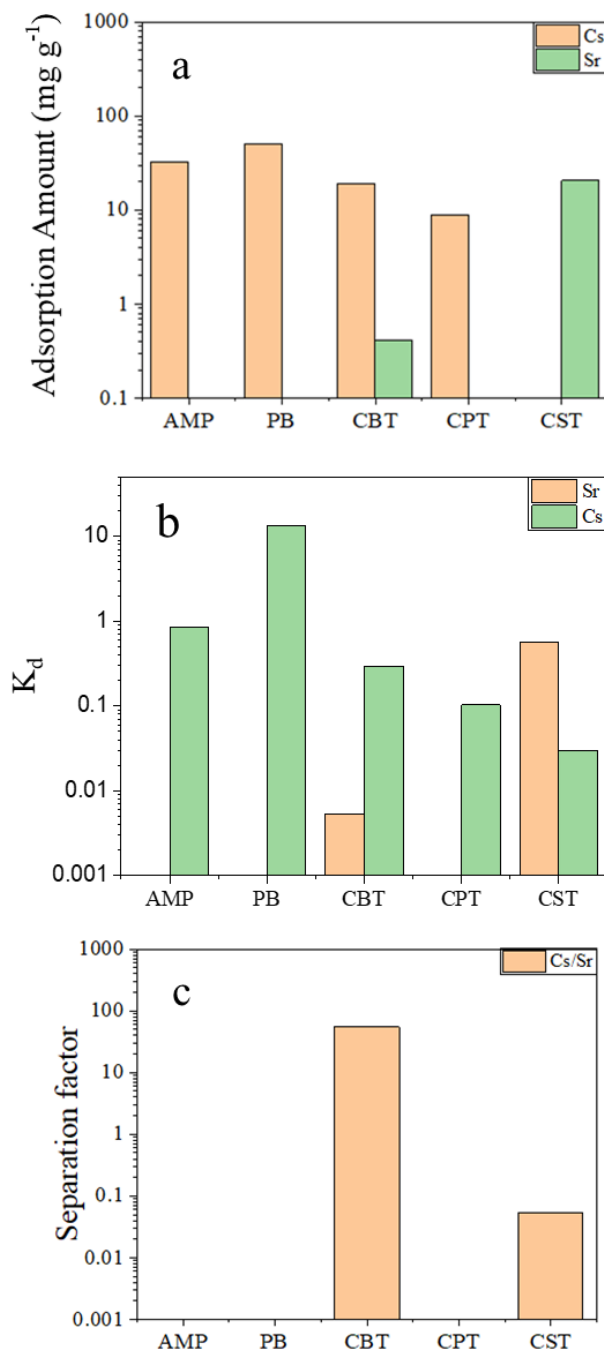


Figure 4. (a). Adsorption amount of adsorbents in artificial seawater. (b). Distribution coefficient. (c). Separation factor of strontium and cesium.

To explore the adsorption kinetics, 0.1 g of the adsorbent was added in 50 mL of simulated seawater for adsorption, and the cesium concentration was measured at 2, 5, 8 and 12 h, respectively (Figure 5a). Two commonly used kinetic models were used for kinetic fitting of adsorption. The pseudo-first-order adsorption kinetics is expressed as follows [3]:

$$\log(Q_e - Q_t) = \log Q_e - \frac{k_1 t}{2.303} \tag{6}$$

where Q_e is the equilibrium adsorption capacity of adsorbent for cesium (mg g^{-1}), Q_t is the adsorption capacity at time t , and k_1 is the first order rate constant (min^{-1}). The pseudo-second-order adsorption kinetics is expressed as follows [4]:

$$\frac{t}{Q_t} = \frac{1}{k_2 Q_e^2} + \frac{t}{Q_e} \tag{7}$$

where k_2 is the second-order adsorption rate constant ($\text{g mg}^{-1} \text{min}^{-1}$). Figure 5b shows the linear fitting of $\log(Q_e - Q_t)$ to t , and Figure 5c shows the linear fitting of t/Q_t to t . The results showed that the pseudo-second-order adsorption kinetics can describe the adsorption kinetics well, with k_2 of $0.0070 \text{ g mg}^{-1} \text{min}^{-1}$ (AMP), $5.05 \times 10^{12} \text{ g mg}^{-1} \text{min}^{-1}$ (PB), $0.0789 \text{ g mg}^{-1} \text{min}^{-1}$ (CBT), and $0.020 \text{ g mg}^{-1} \text{min}^{-1}$ (CPT), respectively, indicating that the chemisorption process is the rate control step. For CST, the pseudo-first-order adsorption kinetics can better describe the adsorption kinetics, with k_1 of 0.6090 min^{-1} .

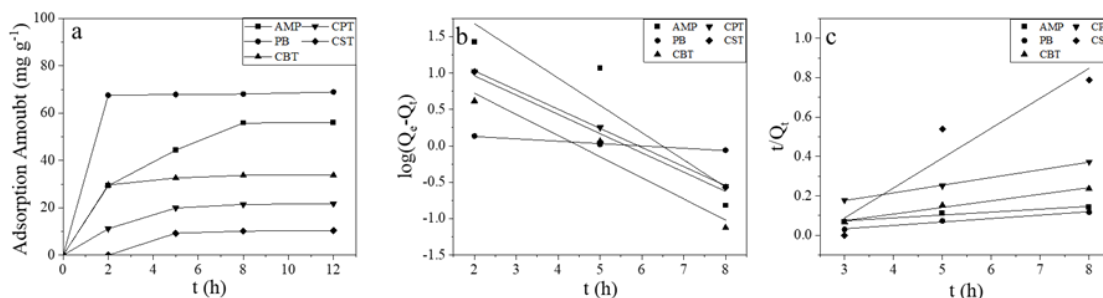


Figure 5. (a). Adsorption amounts with time (b). Fitting of pseudo-first-order dynamics model, (c). Fitting of pseudo-second-order dynamics model.

3.4. Adsorption in Salt Lake Brine

The concentration of Li, Na, K, Rb and Cs in salt lake brine is 5488, 1879.5, 763.5, 0.0331 and 0.0305 mg L^{-1} , and the ratio of Li, Na, K and Rb to Cs in brine is 179,934, 61,623, 25,033 and 1.09, respectively.

As shown in Figure 6, after 12 h adsorption by AMP, the adsorption amount of Li, Rb and Cs is 67.25, 0.00255 and 0.0064 mg g^{-1} , respectively. The adsorbed amount ratios of Li and Rb to Cs after AMP adsorption are 10,507.81 and 0.40, indicating that AMP had a strong selectivity for Cs. The distribution coefficients of Li, Rb and Cs (adsorbent to salt lake brine) are 0.0126, 0.0911 and 0.3616, respectively. The distribution coefficients of Cs are significantly higher than those of other ions, indicating that the adsorbent has a better enrichment effect on Cs. The separation factor of Cs to Li is 28.78, and Cs to Rb is 3.97.

For PB, after adsorption for 12 h, the adsorption amount of Li, Na, K, Rb and Cs is 44.75, 18.25, 2.68, 0.00525 and 0.011 mg g^{-1} , and the residual concentrations of Li, Na, K, Rb and Cs in brine are 778, 80.13, 19.44, 2.64×10^{-4} and $6.40 \times 10^{-5} \text{ mg L}^{-1}$, respectively. The ratio of adsorbed Li, Na and K to Cs on PB decreases to 4068, 1659 and 243, respectively, indicating that Cs is enriched greatly by PB. The distribution coefficients of Li, Na, K, Rb and Cs in adsorbent to brine are 0.0081, 0.0099, 0.0035, 0.2323 and 1.2941, respectively. The separation factors of Cs to Li, Na, K and Rb are 156.12, 130.69, 366.78 and 5.57, respectively.

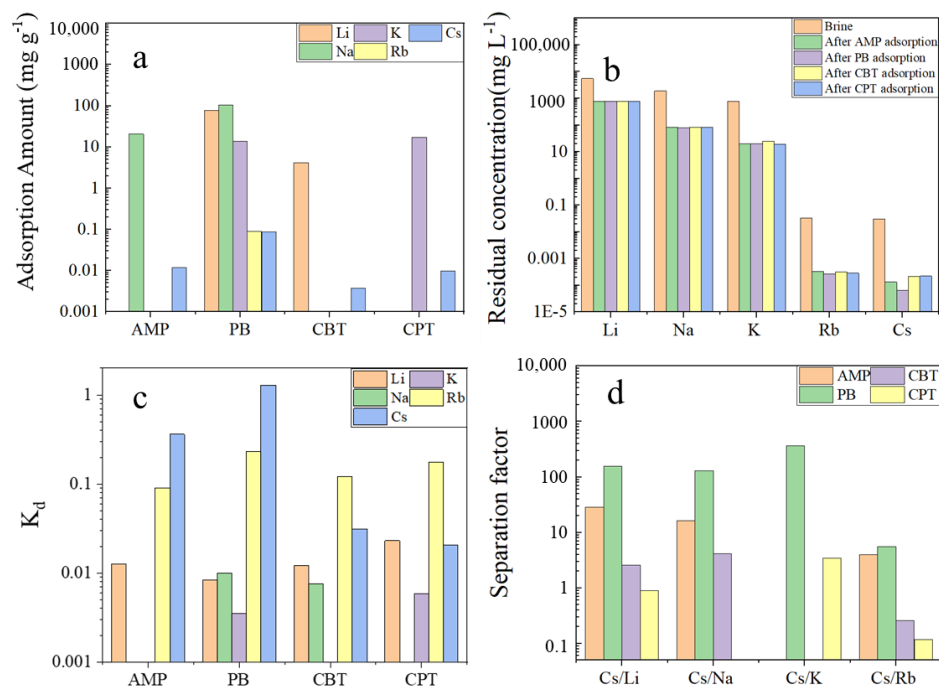


Figure 6. (a). Adsorption amount of adsorbents in brine (b). Residual concentration of ions in the solution after adsorption (c). Distribution coefficient of ions (d). Separation factor of cesium to other ions.

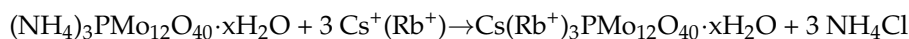
After 12 h adsorption by chabazite, the adsorption amounts of Li, Na, Rb and Cs are 64.75, 14, 0.00325 and 0.0009 mg g⁻¹, respectively. The adsorbed amount ratios of Li, Na and Rb to Cs are 71,944.44, 15,555.56 and 3.61, respectively. The distribution coefficients of Li, Na, Rb and Cs on adsorbent to brine are 0.0121, 0.0076, 0.1222 and 0.0314, respectively. From the analysis of the distribution coefficient, the enrichment of Cs by chabazite is relatively small. The separation factors of Cs on Li, Na and Rb are 2.60, 4.15 and 0.26, respectively.

After 12 h of adsorption by clinoptilolite, the adsorption amount of Li, K, Rb and Cs are 121, 4.45, 0.0043 and 0.0006 mg g⁻¹, respectively. The residual concentrations of Li, Na, K, Rb and Cs are 756, 82.59, 19.35, 2.87 × 10⁻⁴, 2.21 × 10⁻⁴ mg L⁻¹, respectively. The adsorbed amount ratio of Cs to Li, K and Rb is 201,666.67, 7416.67, 7.17. The distribution coefficients of Li, K, Rb and Cs are 0.0231, 0.0059, 0.1755 and 0.0205, respectively. The distribution coefficient shows that the selection and enrichment of Cs by clinoptilolite is not obvious. The separation factors of Cs for Li, K and Rb are 0.89, 3.47 and 0.12, respectively.

It can be observed that, in brine, the order of adsorption amount is as follows: PB (0.011 mg g⁻¹) > AMP (0.0064 mg g⁻¹) > CBT (0.0009 mg g⁻¹) > CPT (0.0006 mg g⁻¹). The adsorption amount and separation factor of PB for Cs are the most excellent, followed by AMP and CBT. The low adsorption amount is related to the trace Cs⁺ (0.0305 mg L⁻¹) and interference of other ions in brine.

3.5. Adsorption Mechanism

Figure 7 shows the structure of adsorbents. In AMP, [PM₁₂O₄₀] is 1:12A heteropoly anion with a Keggin structure. NH₄⁺ is filled in the gap formed by the anion PM₁₂O₄₀³⁻, and NH₄⁺ can exchange with ions (e.g., Cs⁺) in solution. The equation is expressed as follows [24,25]:



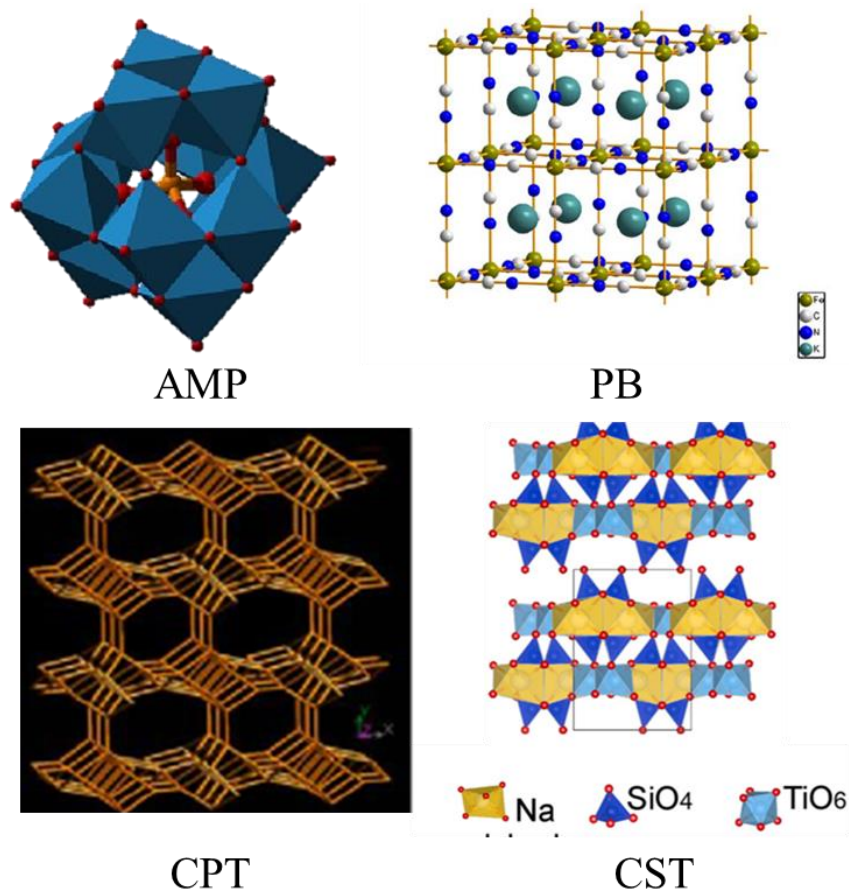


Figure 7. Schematic diagram of adsorbents structure.

The adsorption of cesium by PB is controlled by three mechanisms [26]: ion exchange between potassium ion and cesium ion, surface vacancy adsorption for cesium ion, and chemical adsorption at the hydrophilic lattice defect sites, in which the protons are displaced from the coordination water. The chabazite possesses an eight-element ring channel structure with a pore size of 3.8 Å and a pore volume of approximately 0.42 cm³ g⁻¹. The presence of tetrahedral aluminum makes it negatively charged and can exchange cations in solution [19]. Clinoptilolite has a relatively open pore structure. When it is in contact with some metal salt solution, part of the cation in the clinoptilolite pore can be exchanged with the metal cation in the solution without causing damage to the tetrahedral structure of clinoptilolite. The modification of natural clinoptilolite with sodium chloride can provide more active sites for Cs⁺ adsorption [27]. The ideal molecular formula of sodium titanium silicate is Na₂Ti₂O₃(SiO₄)₂H₂O. The frame structure is composed of TiO₆ octahedron and SiO₄ tetrahedron, with a special pore structure, which has a strong ion adsorption performance and strong irradiation stability. It has good selectivity for Sr in acidic, neutral and alkaline solutions [28].

For ion exchange adsorption of adsorbents, the potential of the cation in solution (i.e., the ratio of charge to radius of the hydrated ion, Z/r) determines the interaction force between the adsorbents and ions. Table 1 shows the hydration radius and potential of ions. Thus, the order of selectivity in dilute solution is Sr²⁺, Ca²⁺, Mg²⁺, Cs⁺, Rb⁺, K⁺, Na⁺ and Li⁺, which is consistent with the results in mixed solution. With the increase in ionic strength, the shielding effect of ions on surface charge of adsorbent is enhanced. Thus, multiple adsorption mechanisms of PB favor the selective adsorption in complex solutions. Table 2 gives the adsorption performance of some typical adsorbents for Cs⁺.

Table 1. The hydration radius and potential of the ions.

Ion	Ionic Hydration Radius/Å	Electron Charge/Z	Potential/(Z/r)
Li ⁺	3.82	1	0.262
Na ⁺	3.58	1	0.279
K ⁺	3.31	1	0.302
Rb ⁺	3.29	1	0.304
Cs ⁺	3.29	1	0.304
Ca ²⁺	4.12	2	0.485
Mg ²⁺	4.28	2	0.467
Sr ²⁺	4.12	2	0.485

Table 2. Some typical adsorbents for Cs⁺.

Adsorbent	Solution Composition	Adsorption Performance for Cs ⁺	Ref.
AMP	CsCl (1 mg L ⁻¹)	Q _e 8.49 mg g ⁻¹	[28]
AMP	Salt lake brine	Q _e 0.0064 mg g ⁻¹	This work
PB	CsCl (900 mg L ⁻¹)	Q _e 42.46 mg g ⁻¹	[29]
PB on PAN membrane	Alkaline metal mixed solution (1 mmol L ⁻¹)	Q _e 94.9 mg g ⁻¹	[3]
PB	Salt lake brine	Q _e 0.011 mg g ⁻¹	This work
Chabazite	CsCl (86 mg L ⁻¹)	Q _e 370 mg g ⁻¹	[30]
Chabazite	Mixed solution (1 mmol L ⁻¹)	Q _e 50.51 mg g ⁻¹	This work
Clinoptilolite	CsCl (649 mg L ⁻¹)	Q _e 122.7 mg g ⁻¹	[31]
Modified Clinoptilolite	Mixed solution (1 mmol L ⁻¹)	Q _e 42.97 mg g ⁻¹	This work
CST	CsCl (330 mg L ⁻¹)	Q _e 194 mg g ⁻¹	[32]
CST	Mixed solution (1 mmol L ⁻¹)	Q _e 13.41 mg g ⁻¹	This work

It should be noted that other issues such as price, stability and reusability of adsorbents, etc., also should be considered in applications. For example, CST is chemically, thermally, and radiation stable, and is highly effective for removing cesium from highly alkaline (pH > 14), neutral and acidic solutions, and for removing strontium from basic and neutral solutions. However, the cesium adsorption is described as a non-elutable ion exchange, and it is not practical to recycle the CST [33].

4. Conclusions

The adsorption of cesium and strontium on ammonium phosphomolybdate, Prussian blue, chabazite, clinoptilolite and titanium silicate was investigated under the same conditions. In the mixed solution, the adsorption amount of ammonium phosphomolybdate for cesium is the largest, and Prussian blue shows the best selection for cesium. In the artificial seawater and salt lake brine, Prussian blue displays the highest adsorption amount and an excellent selectivity for cesium. In salt lake brine, the separation factor of Cs to Li, Na, K and Rb is 156.12, 130.69, 366.78 and 5.57, respectively. Multiple adsorption mechanisms favor the selective adsorption of PB in complex solutions. These results provide useful information for choosing adsorbents for cesium and strontium in applications.

Author Contributions: Conceptualization, Z.J., Y.Y. and L.H.; methodology, Z.J. and S.F.; software, Z.J. and S.F.; validation, Z.J., Y.Y. and S.F.; formal analysis, S.F.; investigation, Z.J. and S.F.; resources, Z.J., Y.Y. and L.H.; data curation, S.F.; writing—original draft preparation, S.F.; writing—review and editing, Z.J., Y.Y. and L.J.; visualization, S.F.; supervision, Z.J.; project administration, Z.J. and Y.Y.; funding acquisition, Z.J. and Y.Y. All authors have read and agreed to the published version of the manuscript.

Funding: This work was supported by the National Natural Science Foundation of China (No. 51920105012), and the National Natural Science Foundation of China and Qinghai Qaidam Saline Lake Chemical Science Research Joint Fund.

Informed Consent Statement: Not applicable.

Data Availability Statement: Not applicable.

Conflicts of Interest: The authors declare no conflict of interest.

References

1. Qian, J.; Han, X.; Yang, S.; Kuang, L.; Hua, D. A strategy for effective cesium adsorption from aqueous solution by poly(pentacyanoferrate)-grafted polypropylene fabric under gamma-ray irradiation. *J. Taiwan Inst. Chem. Eng.* **2018**, *89*, 162–168. [[CrossRef](#)]
2. Qian, J.; Cai, S.; Yang, S.; Hua, D. A thermo-sensitive polymer network crosslinked by Prussian blue nanocrystals for cesium adsorption from aqueous solution with large capacity. *J. Mater. Chem. A* **2017**, *5*, 22380–22388. [[CrossRef](#)]
3. Jia, Z.; Cheng, X.; Guo, Y.; Tu, L. In-situ preparation of iron (III) hexacyanoferrate nano-layer on polyacrylonitrile membranes for cesium adsorption from aqueous solutions. *Chem. Eng. J.* **2017**, *325*, 513–520. [[CrossRef](#)]
4. Zhiqian, J.; Shuang, H.; Xiaoxue, C.; Xiaoyu, L.; Lanying, T. Fabrication of Prussian blue/polydopamine layers on polyacrylonitrile membranes for efficient adsorption of cesium. *Desalination Water Treat.* **2019**, *163*, 125–132.
5. Jia, Z.; Sun, G. Preparation of prussian blue nanoparticles with single precursor. *Colloids Surf. A Physicochem. Eng. Asp.* **2007**, *302*, 326–329. [[CrossRef](#)]
6. Jia, Z. Synthesis of Prussian Blue nanocrystals with metal complexes as precursors: Quantitative calculations of species distribution and its effects on particles size. *Colloids Surf. A Physicochem. Eng. Asp.* **2011**, *389*, 144–148. [[CrossRef](#)]
7. Jang, J.; Lee, D.S. Enhanced adsorption of cesium on PVA-alginate encapsulated Prussian blue-graphene oxide hydrogel beads in a fixed-bed column system. *Bioresour. Technol.* **2016**, *218*, 294–300. [[CrossRef](#)]
8. Aulia, A.H.; Kuk, C. Selective adsorption of cesium from an aqueous solution by a montmorillonite-Prussian blue hybrid. *Chem. Eng. J.* **2018**, *349*, 595–602.
9. Yin, J.; Yang, S.; He, W.; Zhao, T.; Hua, D. Biogene-derived Aerogels for Simultaneously Selective Adsorption of Uranium(VI) and Strontium(II) by Co-imprinting Method. *Sep. Purif. Technol.* **2021**, *271*, 118849–118858. [[CrossRef](#)]
10. Ilhan, S.; Kahruman, C.; Yusufoglu, I. Characterization of the thermal decomposition products of ammonium phosphomolybdate hydrate. *J. Anal. Appl. Pyrolysis* **2007**, *78*, 363–370. [[CrossRef](#)]
11. Wei, J.; Tao, W.C.; Hao, C.B.; Xian, S.B.; Ji, B.; Wz, A.; Hl, A.; Sheng, D. Room temperature synthesis of high-entropy Prussian blue analogues. *Nano Energy* **2021**, *79*, 105464–105471.
12. Metwally, S.S.; Attallah, M.F. Impact of surface modification of chabazite on the sorption of iodine and molybdenum radioisotopes from liquid phase. *J. Mol. Liq.* **2019**, *290*, 111237. [[CrossRef](#)]
13. Prajitno, M.Y.; Tangparitkul, S.; Zhang, H.; Harbottle, D.; Hunter, T.N. The effect of cationic surfactants on improving natural clinoptilolite for the flotation of cesium. *J. Hazard. Mater.* **2020**, *402*, 123567. [[CrossRef](#)] [[PubMed](#)]
14. Kholdeeva, O.A.; Trukhan, N.N. Mesoporous titanium silicates as catalysts for the liquid-phase selective oxidation of organic compounds. *Russ. Chem. Rev.* **2006**, *75*, 411–432. [[CrossRef](#)]
15. Hijikata, T.; Uozumi, K.; Tsukada, T.; Koyama, T.; Ishikawa, K.; Ono, S.; Suzuki, S.; Denton, M.; Raymont, J. Early construction and operation of the highly contaminated water treatment system in Fukushima Daiichi Nuclear Power Station (II)—Dynamic characteristics of KURION media for Cs removal in simulated contaminated water. *J. Nucl. Sci. Technol.* **2014**, *51*, 894–905. [[CrossRef](#)]
16. Yamagishi, I.; Nagaishi, R.; Kato, C.; Morita, K.; Denton, M. Characterization and storage of radioactive zeolite waste. *J. Nucl. Sci. Technol.* **2014**, *51*, 1044–1053. [[CrossRef](#)]
17. Antonello, A.; Benedetti, C.; Pérez-Pla, F.F.; Kokkinopoulou, M.; Kirchoff, K.; Fischer, V.; Landfester, K.; Gross, S.; Munoz-Espi, R. Colloidally confined crystallization of highly efficient ammonium phosphomolybdate catalysts. *ACS Appl. Mater. Interfaces* **2018**, *10*, 23174–23186. [[CrossRef](#)]
18. Farah, A.M.; Shooto, N.D.; Thema, F.T.; Modise, J.S.; Dikio, E.D. Fabrication of prussian blue/multi-walled carbon nanotubes modified glassy carbon electrode for electrochemical detection of hydrogen peroxide. *Int. J. Electrochem. Sci.* **2012**, *7*, 4302–4313.
19. Prakash, A.M.; Unnikrishnan, S. Synthesis of SAPO-34: High silicon incorporation in the presence of morpholine as template. *J. Chem. Soc. Faraday Trans.* **1994**, *90*, 2291–2296. [[CrossRef](#)]
20. Wang, R.; Luo, Z.; Tan, Q.; Wang, R.; Xiao, Z. Sol-gel hydrothermal synthesis of nano crystalline silicotitanate and its strontium and cesium adsorption. *Environ. Sci. Pollut. Res.* **2020**, *27*, 4404–4413. [[CrossRef](#)]
21. Lim, D.J.; Marks, N.A.; Rowles, M.R. Universal Scherrer equation for graphene fragments. *Carbon* **2020**, *162*, 475–480. [[CrossRef](#)]
22. Franus, W.; Wdowin, M.; Franus, M. Synthesis and characterization of zeolites prepared from industrial fly ash. *Environ. Monit. Assess.* **2014**, *186*, 5721–5729. [[CrossRef](#)]
23. Solbr, S.; Allison, N.; Waite, S.; Mikhailovsky, S.V.; Bortun, A.I.; Bortun, L.N.; Clearfield, A. Cesium and Strontium Ion Exchange on the Framework Titanium Silicate $M_2Ti_2O_3SiO_4 \cdot nH_2O$ ($M = H, Na$). *Environ. Sci. Technol.* **2001**, *35*, 626–629. [[CrossRef](#)] [[PubMed](#)]

24. Scheidhauer, J.; Messainguiral, L. Separation and measurement of cesium 137 and Barium 137 in Radioactive effluents. *Chim. Anal. Merged Method. Phys. Anal. Analysis* **1964**, *46*.
25. Smit, J.; Jacobs, J.J.; Robb, W. Cation exchange properties of the ammonium heteropolyacid salts. *J. Inorg. Nucl. Chem.* **1959**, *12*, 95–103. [[CrossRef](#)]
26. Wi, H.; Kim, H.; Oh, D.; Bae, S.; Hwang, Y. Surface modification of poly(vinyl alcohol) sponge by acrylic acid to immobilize Prussian blue for selective adsorption of aqueous cesium. *Chemosphere* **2019**, *226*, 173–182. [[CrossRef](#)]
27. Philip, C.V.; Kim, S.H.; Philip, M.; Anthony, R.G. The Effect of Hydrogen Peroxide on a CST Under Cesium Ion Exchange Conditions. *Sep. Sci. Technol.* **2003**, *38*, 3009–3029. [[CrossRef](#)]
28. Ma, G.; Zheng, Y.; Zhou, Y.; Gao, L.; Liu, B.; Yu, X.; Zhang, L. Ammonium molybdophosphate functionalized copolymer micelles for efficient Cs⁺ adsorption. *J. Polym. Res.* **2021**, *28*, 465. [[CrossRef](#)]
29. Chen, G.-R.; Chang, Y.-R.; Liu, X.; Kawamoto, T.; Tanaka, H.; Kitajima, A.; Parajuli, D.; Takasaki, M.; Yoshino, K.; Chen, M.-L.; et al. Prussian blue (PB) granules for cesium (Cs) removal from drinking water. *Sep. Purif. Technol.* **2015**, *143*, 146–151. [[CrossRef](#)]
30. Yang, H.-M.; Park, C.W.; Kim, I.; Yoon, I.-H.; Sihm, Y. Sulfur-modified chabazite as a low-cost ion exchanger for the highly selective and simultaneous removal of cesium and strontium. *Appl. Surf. Sci.* **2020**, *536*, 147776–147786. [[CrossRef](#)]
31. Lihareva, N.; Petrov, O.; Dimowa, L.; Tzvetanova, Y.; Piroeva, I.; Ublekov, F.; Nikolov, A. Ion exchange of Cs⁺ and Sr²⁺ by natural clinoptilolite from bi-cationic solutions and XRD control of their structural positioning. *J. Radioanal. Nucl. Chem.* **2020**, *323*, 1093–1102. [[CrossRef](#)]
32. Ding, D.; Li, K.; Fang, D.; Ye, X.; Hu, Y.; Tan, X.; Liu, H.; Wu, Z. Novel Biomass-Derived Adsorbents Grafted Sodium Titanium Silicate with High Adsorption Capacity for Rb⁺ and Cs⁺ in the Brine. *ChemistrySelect* **2019**, *4*, 13630–13637. [[CrossRef](#)]
33. National Academies of Sciences, Engineering, and Medicine. *Alternatives for High-Level Waste Salt Processing at the Savannah River Site*; The National Academies Press: Washington, DC, USA, 2000.

Disclaimer/Publisher's Note: The statements, opinions and data contained in all publications are solely those of the individual author(s) and contributor(s) and not of MDPI and/or the editor(s). MDPI and/or the editor(s) disclaim responsibility for any injury to people or property resulting from any ideas, methods, instructions or products referred to in the content.